# Metal Halide Perovskite for next-generation optoelectronics: progresses and prospects

He Dong[1†], Chenxin Ran[1*†], Weiyin Gao[1], Mingjie Li[4,5], Yingdong Xia[2*] and Wei Huang[1,2,3*] [ID]

**Abstract**

Metal halide perovskites (MHPs), emerging as innovative and promising semiconductor materials with prominent optoelectronic properties, has been pioneering a new era of light management (ranging from emission, absorption, modulation, to transmission) for next-generation optoelectronic technology. Notably, the exploration of fundamental characteristics of MHPs and their devices is the main research theme during the past decade, while in the next decade, it will be primarily critical to promote their implantation in the next-generation optoelectronics. In this review, we first retrospect the historical research milestones of MHPs and their optoelectronic devices. Thereafter, we introduce the origin of the unique optoelectronic features of MHPs, based on which we highlight the tunability of these features via regulating the phase, dimensionality, composition, and geometry of MHPs. Then, we show that owing to the convenient property control of MHPs, various optoelectronic devices with target performance can be designed. At last, we emphasize on the revolutionary applications of MHPs-based devices on the existing optoelectronic systems. This review demonstrates the key role of MHPs played in the development of modern optoelectronics, which is expected to inspire the novel research directions of MHPs and promote the widespread applications of MHPs in the next-generation optoelectronics.

**Keywords:** Metal halide perovskites, Optoelectronic characteristics, Optoelectronic devices, Revolutionary applications

## 1 Introduction

Metal halide perovskites (MHPs) have been emerging as the rising star in the field of optoelectronics during the past decade, and the state-of-the-art optoelectronic technologies based on MHPs, such as perovskite solar cells (PSCs), light emitting diodes (LEDs), photodetectors (PDs) and lasers, have been leading the prevailing paradigm owing to the intriguing optoelectronic properties of MHPs. MHPs family, taking the general formula of $ABX_3$ ($A = CH_3NH_3^+$ (MA), $HC(NH_2)_2^+$ (FA), and $Cs^+$, $B = Pb^{2+}$, $Sn^{2+}$, $X = I^-$, $Cl^-$, $Br^-$), possesses the merits of facile and low-cost processing and the favorable attributes of tunable optical and electronic features, providing a rich and fertile ground for the development of high-performing multifunctional optoelectronic devices and their future industrialization.

The first study of optoelectronics of MHPs could be traced back to 1950s, the intensely colored crystals of $CsPbX_3$ ($X = Cl$, Br) with perovskite structure exhibits the behavior of frequency-dependent photoconductive response, implying the special electrical properties of perovskites [1]. Shortly thereafter in early 1990s, Mitzi and co-workers focused particular interest on the layered tin halide perovskites that are naturally self-assembled into quantum confinement structures (QWS) in the presence of alkylammonium cations,

---

†He Dong and Chenxin Ran equally contributed to this work

*Correspondence: iamcxran@nwpu.edu.cn; iamydxia@njtech.edu.cn; iamdirector@fudan.edu.cn

[1] Frontiers Science Center for Flexible Electronics, Xi'an Institute of Flexible Electronics (IFE) and Xi'an Institute of Biomedical Materials & Engineering, Northwestern Polytechnical University, Xi'an 710072, China
[2] Key Laboratory of Flexible Electronics (KLOFE) & Institution of Advanced Materials (IAM), Nanjing Tech University (NanjingTech), Nanjing 211816, Jiangsu, China
Full list of author information is available at the end of the article

exhibiting obvious excitonic features and demonstrating potential application in LEDs and transistors [2], crucially with the interesting electronic properties and ability by tuning the MHP structures flexibly [3–5]. In the meanwhile, the first observation of light emission and lasing in $(C_6H_{13}NH_3)_2PbI_4$ was reported in 1998 [6]. Subsequently, as the birth of first perovskite-sensitized solar cell with a power conversion efficiency (PCE) of 3.8% in 2009 [7], "perovskite fever" with a focus on solar cells application makes several milestones in PCE improvement, which has exceeded 20% since then [8]. This breakthrough process triggers the researchers' curiosity to explore the intrinsic optoelectronic properties of MHPs, where the adjustable band gap, long carrier diffusion length, strong light absorption, low defect density and solution processability are identified [9]. In the mild-2010s, MHPs are shown to be promising for optical sources with the high optical gain and stable amplified spontaneous emission (ASE) with a threshold of $10\pm2\ \mu J\ cm^{-2}$ at room temperature [10], and the first laser work in the field without external cavity [11] as well as the first optically pumped perovskite microcavity laser were reported shortly after [12]. In 2015, the first ASE and lasing in MHP nanocrystals of $CsPbX_3$ was demonstrated with low pump thresholds down to $5\pm2\ \mu J\ cm^{-2}$ [13]. Almost the same time, the first room temperature perovskite LEDs (external quantum efficiency (EQE) $\sim 0.76\%$) were reported by Friend and co-workers [14]. Meanwhile, the first $MAPbI_3$ PDs with X-ray sensitivity of 25 $\mu C\ mGy_{air}^{-1}\ cm^{-3}$ was investigated by Heiss and co-workers [15], Park and co-workers then achieved highly sensitive X-ray PDs up to

11 $\mu C\ mGy_{air}^{-1}\ cm^{-2}$ based on printable $MAPbI_3$ films in 2017 [16]. The next evolution of MHPs in optoelectronics comes from the revival of layered perovskites and perovskite nanocrystals (NCs) in late 2010s, and they have shown competitive photoluminescence (PL) and electroluminescence (EL) efficiency compared with bulk perovskites [17], pushing the related studies, especially of the relationships between dimensionality, size, geometry, composition, colloidal synthesis approaches and their optoelectronic properties to a new upsurge, in which the EQE of green, red, and near-infrared LEDs can be as high as 20.3%, 21.3% and 21.6% [18–20], respectively. Also, new breakthrough in $CsPbBr_3$ NCs X-ray detectors has been made with a low dose rate of 13 nGy s$^{-1}$ [21]. Propelling current interest in the 2020s is that MHPs continue to exhibit new and surprising optoelectronic properties, the certified PCE for single-junction PSCs, all-perovskite tandem solar cells and hybrid tandem PSCs has been up to 25.7%, 28% and 31.3%, respectively [22], and new applications of this materials expand not only to PSCs, LEDs and PDs, but also to facilitate the integration of optoelectronic devices. Meanwhile, the challenges such as instability bottleneck has been gradually resolved. One can say that the optoelectronic properties of these materials create a host of new avenues for the scientific community to explore. Figure 1 demonstrates the representative progresses of MHPs for optoelectronics. Inspiringly, solid researches have been carried out during the course of development to disclose the unique optoelectronic features of MHPs, and their multidiscipline applications have given new momentum to



**Fig.1** Representative progresses of MHPs for optoelectronics
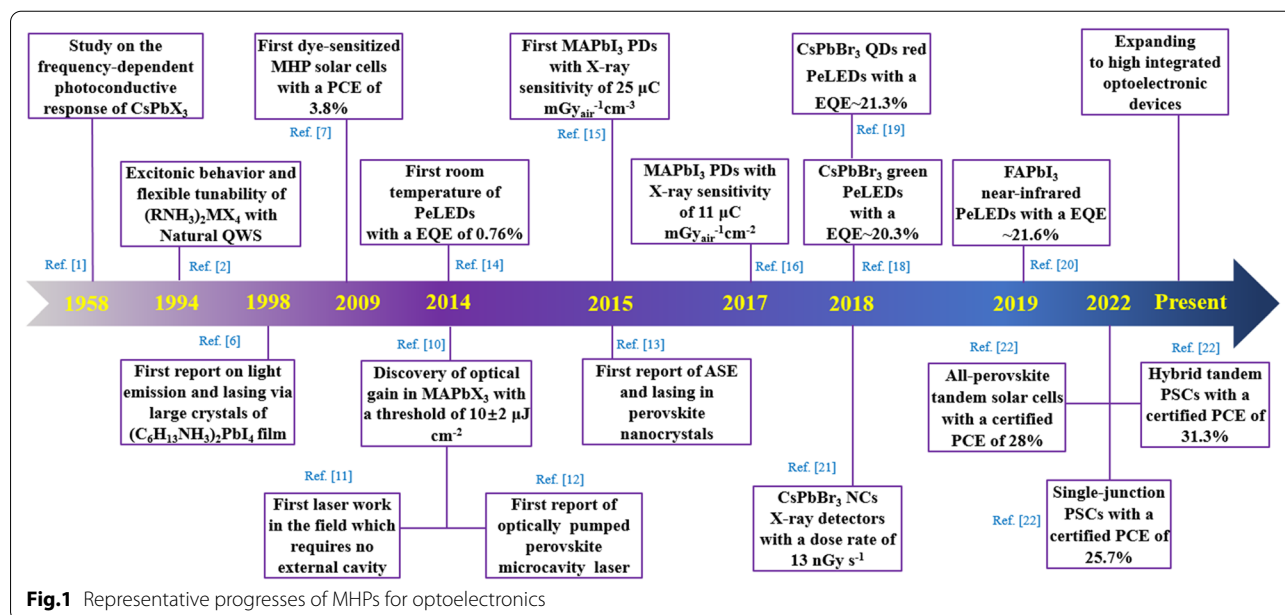
the field of optoelectronics, enabling the rapid revolutionary step towards their practical use for human civilization.
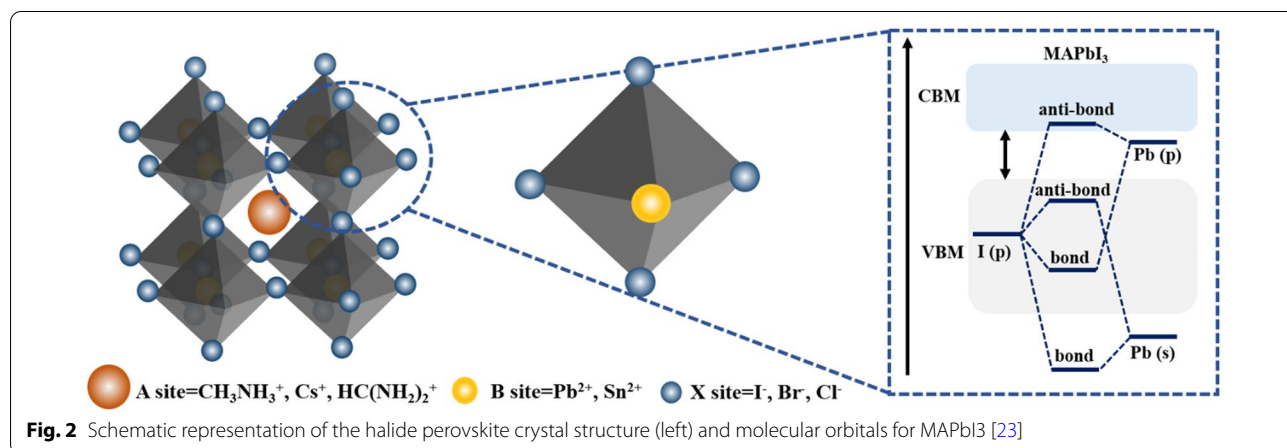
In this review, we dedicate to giving a panorama picture on the optoelectronic traits of MHPs and their revolutionary impact on the next-generation optoelectronics. We first introduce the structure of MHPs and the origin of their optoelectronic properties, and briefly discuss the relationship between structure and optoelectronic properties of MHPs. Then, we summarize the merits of MHPs by focusing on the fine controlling of the optoelectronic properties by regulating the structure of MHPs, including phase, dimensionality, composition, and geometry. Thereafter, we highlight the revolutionary applications of MHPs in the technologies that are related to important area of human society, which includes functional integration system, information display system, electronic communication system, and health & medical system. This perspective aims at providing critical guidance for inspiring the novel research directions of MHPs to promote the widespread application of MHPs in optoelectronics.

## 2 Origin of optoelectronic properties of MHPs

In a typical $ABX_3$ perovskite, B occupies the center of an octahedral $[BX_6]^{4-}$ cluster, which forms corner-shared octahedral $BX_6$ framework, while A is 12-fold cuboctahedral coordinated with X anions and occupies the interspace of octahedral $BX_6$ framework, as shown in Fig. 2. For $[PbI_6]^{4-}$ in particular, the valence band maximum (VBM) is formed by antibonding orbitals originating from Pb(6 s) and I(5p) atomic states, while antibonding Pb(6p) and I(5 s) orbitals form the conduction band minimum (CBM). Of critical importance, intrinsic electronic configurations of MHPs are the direct origin of their unique optoelectronic properties, including high optical absorption, high carrier mobility, high defect tolerances,

long diffusion lengths, unique ambipolar charge transport, and flexible turnability.

(i) High optical absorption. The high symmetry of $MAPbI_3$ crystal structure leads to direct band gap while the lone pair electrons on Pb *s* orbital results in p-p electronic transitions from VB to CB, contributing to exceptionally high optical absorption of the material [24]. (ii) High carrier mobility. The inorganic Pb-I framework in MHPs mainly contributes to the valence and conduction band-edge state, and both VB and CB of MHPs exhibit antibonding character, and the anti-bonding interaction results in a rather small effective electron mass, enabling the high charge carrier mobility of MHP with the values of tens of $cm^2/(Vs)$ [25, 26]. (iii) High defect tolerance. On the one hand, orbital expands VB bandwidth and raises VB edge, suggesting that most defect states are located within or closer to VB edge. On the other hand, coupling between Pb 6p orbital and I 5p orbital is very weak, and thus CB edge exhibits an ionic character, suggesting that the energy states are not much affected by external defect levels. Therefore, MHPs show high defect-tolerance [27]. (iv) Long diffusion lengths. Long diffusion lengths in MHPs is ascribed from the high carrier mobility and high defect tolerance, and thus the ideal perovskite crystal structure shows long carrier diffusion length greater than 10 μm [28]. (v) Ambipolar charge transport. Because the electron effective mass of MHPs ($0.23m_0$) is considerably balance with hole effective mass ($0.29m_0$), MHPs exhibit unique ambipolar charge transport property, which play an important role in photovoltaic application [29]. (vi) Flexible tunability. Because the band structure is determined by the B and X elements, the substitution of B and/or X gives rise to the feasible tunability of VBM and CBM position as well as the band gap of MHPs. Also, deriving from the doubly bridging halide ion (B-X-B moiety), MHPs possess the unique property of successive phased transition, which can undergo a series



**Fig. 2** Schematic representation of the halide perovskite crystal structure (left) and molecular orbitals for MAPbI3 [23]

of structural changes via changing temperature, pressure, and/or chemistry to force the B-X-B angle deviating from ideal crystal structure [23, 30].

In sum, those unique characteristics of MHPs are derived from their crystal structure and chemical composition, which allows the unprecedented flexibility to independently and synergistically tune the optoelectronic properties of MHPs, laying an important foundation for MHPs being applicable to various optoelectronic applications [31]. In the next section, we will introduce the current understanding on the tunable optoelectronic properties of MHPs.

## 3 Tunable optoelectronic properties of MHPs

### 3.1 Phase transition

The flexible nature of the $BX_6$ framework in $ABX_3$ MHPs is mainly originating from the largest metal-halide-metal (B-X-B) bond angle, providing the perovskites with another interesting property of successive phase transition, which largely influences the electronic st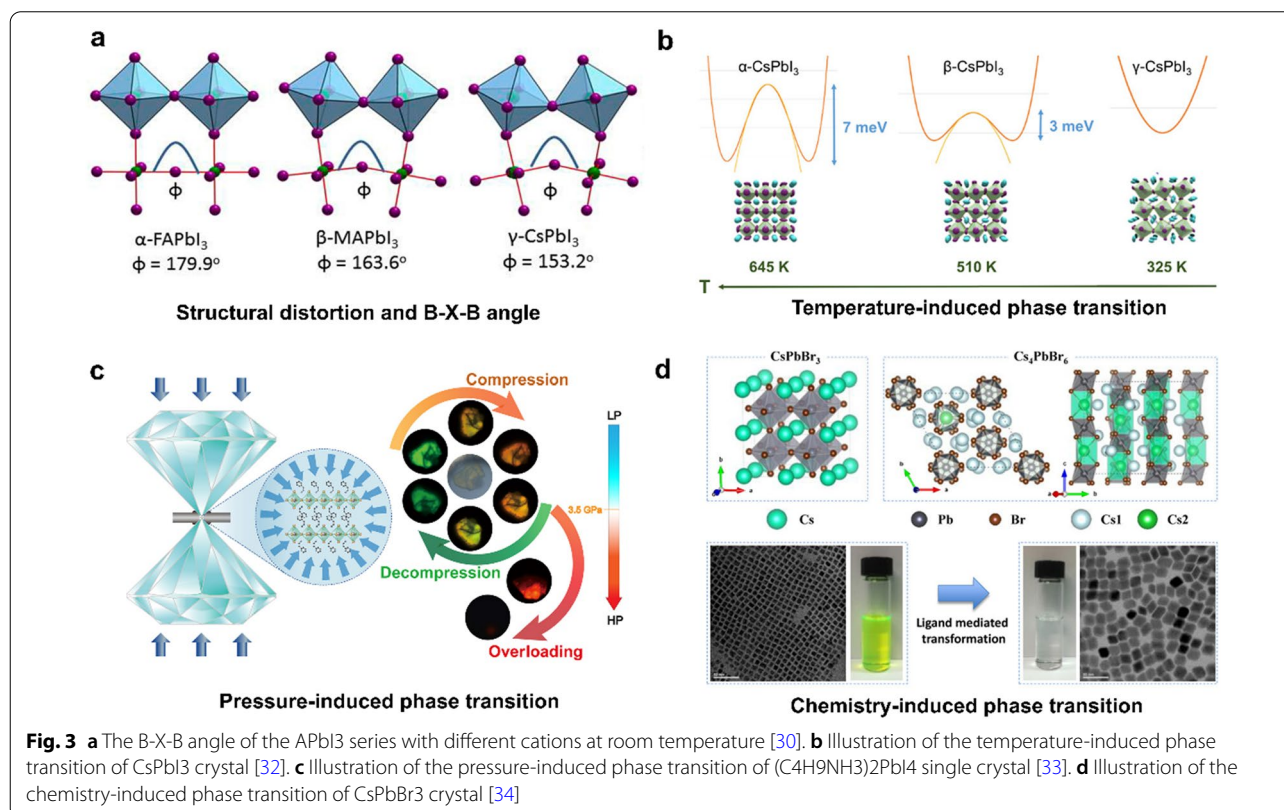ructure and thus the resulting optoelectronic properties of MHPs (Tables 1, 2) [23]. For example, in the prototypical material $APbI_3$, the cation series $MA^+$, $FA^+$ and $Cs^+$ leads to progressively larger octahedral tilting in the perovskite phase at room temperature (Φ change in Fig. 3a) as a result of decreased cation size [30], leading to an increase in band gap from 1.48 eV in α-$FAPbI_3$ to 1.67 eV in γ-$CsPbI_3$. Generally, a series of phase transition of perovskites can be modulated by temperature, pressure and/or chemistry. The structural phase transition of cesium halide perovskites has proven to be controlled by temperature, often between a room temperature non-perovskite phase and a high-temperature perovskite phase (Fig. 3b). These two phases feature distinct optoelectronic properties, such as bandgap, photoluminescence quantum efficiency, charge carrier mobility, and charge carrier lifetime [32]. In addition, the phase transition could also be triggered by high-pressure, and studies have reported that under a few GPa pressure, two-dimensional perovskites (2DPKs) show optical bandgap modulations and enhanced PL effects due to the phase transition. Interestingly, the structure of 2DPK crystals can be stabilized in

**Table 1** Structure phase parameters for typical MHPs

| Composition | Angle length (°) | Angle bond (°) | Crystal system | Space group | Phase transition temperature (K) | Refs. |
|---|---|---|---|---|---|---|
| $FAPbI_3$ | a = b = c = 6.3575 | α = β = γ = 90 | Cubic | *Pm$\bar{3}$m* | α-phase | [35–38] |
| | a = 8.6603 (14); b = 8.6603 (14); | α = β = 90 | Hexagonal | *P6$_3$mc* | δ-phase (423) | |
| | c = 7.9022 (6) | γ = 120 | / | / | Tetragonal, β-phase | |
| | a = 17.7914 (8); b = 17.7914 (8); | α = β = 90 | Trigonal | *P3* | Tetragonal, γ-phase (140) | |
| | c = 10.9016 (6); a = b = 8.98 c = 11.01 | γ = 120 α = β = 90 γ = 120 | Trigonal | *P3m*1 | / | |
| $FAPbBr_3$ | a = b = c = 5.9944 | α = β = γ = 90 | Cubic | *Pm$\bar{3}$m* | / | [36, 39, 40] |
| $MAPbI_3$ | a = b = c = 6.391(1) | α = β = γ = 90 | Cubic | *Pm$\bar{3}$m* | Cubic, α-phase | [35, 41–43] |
| | a = 8.849 (2); b = 8.849 (2); c = 12.642 (10) | α = β = γ = 90 | Tetragonal | *I4cm* | Tetragonal, β-phase (330.4) Orthorhombic, δ-phase, (161.4) | |
| $MAPbBr_3$ | a = b = c = 5.933(2) | α = β = γ = 90 | Cubic | *Pm$\bar{3}$m* | Cubic, α-phase Tetragonal, β-phase (236.3) Tetragonal, γ-phase (155.1) Orthorhombic, δ-phase, (148.8) | [39, 42–44] |
| $MAPbCl_3$ | a = b = c = 5.666(2) | α = β = γ = 90 | Cubic | *Pm$\bar{3}$m* | Cubic, α-phase | [42, 45, 46] |
| | a = 11.1763 (10); b = 11.3409 (10); c = 11.2804 (10) | α = β = γ = 90 | Orthorhombic | *Pnma* | Tetragonal, β-phase (177.2) Orthorhombic, γ-phase (171.5) | |
| $CsPbI_3$ | a = 10.4342 (7); b = 4.7905 (3); c = 17.7610 (10) | α = β = γ = 90 | Orthorhombic | *Pnma* | Cubic, α-phase, Orthorhombic, δ-phase (634) | [35, 47–49] |
| $CsPbCl_3$ | a = b = c = 5.605 | α = β = γ = 90 | Cubic | *Pm$\bar{3}$m* | Cubic Tetragonal (320) Orthorhombic (315) | [50, 51] |
| $CsPbBr_3$ | a = 8.2440 (6); b = 11.7351 (11); c = 8.1982 (8) | α = β = γ = 90 | Orthorhombic | *Pnma* | Cubic Tetragonal (404) Orthorhombic (325) | [35, 47–49, 52] |

**Table 2** Comparison of the key parameters for photodetectors

| Type | Materials structure | Responsivity (mA/W) | Detectivity (Jones) | Excitation wavelength (nm) | Response time | Refs. |
|---|---|---|---|---|---|---|
| Organic–inorganic materials | MAPbI$_3$ polycrystalline film | $2.75 \times 10^5$ | $10^3$ | 830 | 30/20 µs | [53] |
| | Single-crystalline FAPbI$_3$ wafer | $4.5 \times 10^5$ | / | 635 | 8.3/7.5 ms | [54] |
| | MAPbCl$_3$ single crystals | 46.9 | $1.2 \times 10^{10}$ | 365 | 24/62 ms | [45] |
| | MAPbCl$_3$ nanowire arrays | 30 | $10^{10}$ | 450–780 | 20.47/13.81 ms | [55] |
| | MAPbI$_3$ microwire arrays | $1.36 \times 10^4$ | $5.25 \times 10^{12}$ | 420 | 80/240 µs | [56] |
| | MAPbI$_3$/MoS$_2$/APTES | $9.16 \times 10^7$ | $1.29 \times 10^{12}$ | 520 | 6.17/4.5 s | [57] |
| Organic materials | TAPC:C$_{70}$ | 144 | $2.5 \times 10^{13}$ | / | / | [58] |
| | PbPC:C$_{70}$ | / | $4.2 \times 10^{12}$ | 890 | / | [59] |
| | P3HT:PCBM | / | $1.3 \times 10^{12}$ | 445 | / | [60] |
| | ZnO:PPDT2FBT | 150 | $3.0 \times 10^{12}$ | / | / | [61] |
| Inorganic materials | PbS QD | $10^6$ | $1.8 \times 10^{13}$ | 1300 | / | [62] |
| | Graphene-PbS | $10^{10}$ | $7 \times 10^{13}$ | 600 | 10 ms | [63] |



**Fig. 3** **a** The B-X-B angle of the APbI3 series with different cations at room temperature [30]. **b** Illustration of the temperature-induced phase transition of CsPbI3 crystal [32]. **c** Illustration of the pressure-induced phase transition of (C4H9NH3)2PbI4 single crystal [33]. **d** Illustration of the chemistry-induced phase transition of CsPbBr3 crystal [34]

a metastable state or a different phase at ambient pressure after a cycle of compression/decompress and amorphization (above 10 GPa) (Fig. 3c), resulting in a series of the strong excitonic emissions in the PL spectra [33]. Furthermore, through chemical route of acid–base interactions, reversible structural and compositional changes of CsPbX$_3$ nanocrystals can be induced at room temperature between cubic and orthorhombic CsPbX$_3$ (Fig. 3d), which is owing to the controlled self-assembly of small CsPbX$_3$ nanocrystals via the control of the ligand shell environment [34]. These results highlight the potential application of doped halide perovskites in switchable optoelectronics, such as the smart windows, building-integrated photovoltaics (BIPV) and so on.

## 3.2 Dimensionality

Relying on the variety structures and compositions of MHPs, especially in terms of the choice of R cation, the dimensionality of MHPs can be finely tailored from 3D to low-dimensional ones extending from quasi-two- (quasi-2D), two- (2D), one- (1D) to zero- (0D) dimension. Normally, the term "low-dimension" of MHPs is often classified into two types: "structure-level" and "material-level". The "structure-level" low-dimension underlines the morphologies of MHPs, and commonly refers to those nanostructures, such as nanosheet, nanowire, and nanocrystal (Fig. 3a(i)). By contrast, the "material-level" low-dimension emphasizes the intrinsic crystal structure of MHPs, in which the $[BX_6]^{4-}$ octahedra are separated by the bulky dielectric spacer molecules to form bulk assembly of atom-level 0D clusters, 1D quantum wires, or 2D quantum-wells (QWs) (Fig. 4a(ii)). Compared to their 3D counterparts, low-dimensional MHPs possess unique band structures, because the dimensionality and size of the nanostructure have direct consequences on the electronic band gap and joint density of states (DOS) close to the band gap, which is of crucial importance to determine their optoelectronic properties (Fig. 4a(iii)) [64]. Generally, lower dimension MHPs have narrower absorption range owing to their larger bandgaps, which vary with the number of layers (Fig. 4b) [65]. When considering a family of low dimensional MHPs structures composed of the same metal halide octahedral, the lowest energy electronic transition follows the monotonic trend of $E_{g, 3D} < E_{g, 2D} < E_{g, 1D} <$ HOMO–LUMO $_{0D}$. Most importantly, the inclusion of dielectric and quantum confinement effects in low-dimensional MHPs can further increase the discrepancy between the optoelectronic characteristics of 3D and LD structures (Fig. 4c) [66]. The exciton binding energy progressively decreases with the increased *n*, and when n ≤ 2, the perovskites exhibit
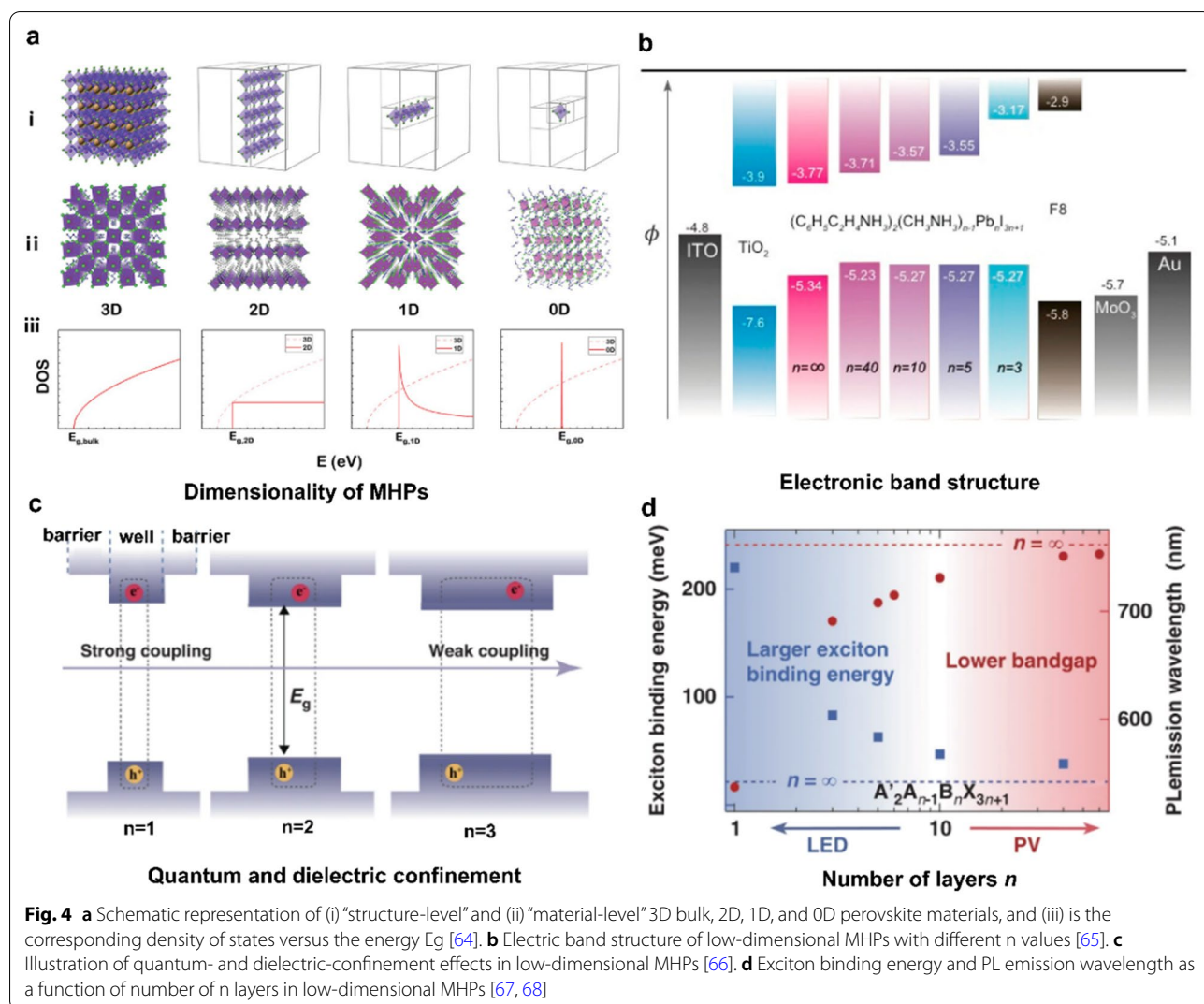


**Fig. 4** **a** Schematic representation of (i) "structure-level" and (ii) "material-level" 3D bulk, 2D, 1D, and 0D perovskite materials, and (iii) is the corresponding density of states versus the energy Eg [64]. **b** Electric band structure of low-dimensional MHPs with different n values [65]. **c** Illustration of quantum- and dielectric-confinement effects in low-dimensional MHPs [66]. **d** Exciton binding energy and PL emission wavelength as a function of number of n layers in low-dimensional MHPs [67, 68]

strong excitonic behavior with high photoluminescence yield (PLQY) at room temperature, and this intensified oscillator strength and optical nonlinearities of low-dimensional MHPs make them suitable for light-emitting applications. While when n ≥ 3, the perovskites have a low exciton binding energy and smaller bandgap, which extends the light absorption range in the visible region, suggesting their suitability of sunlight-to-energy conversion (Fig. 4d) [67, 68].
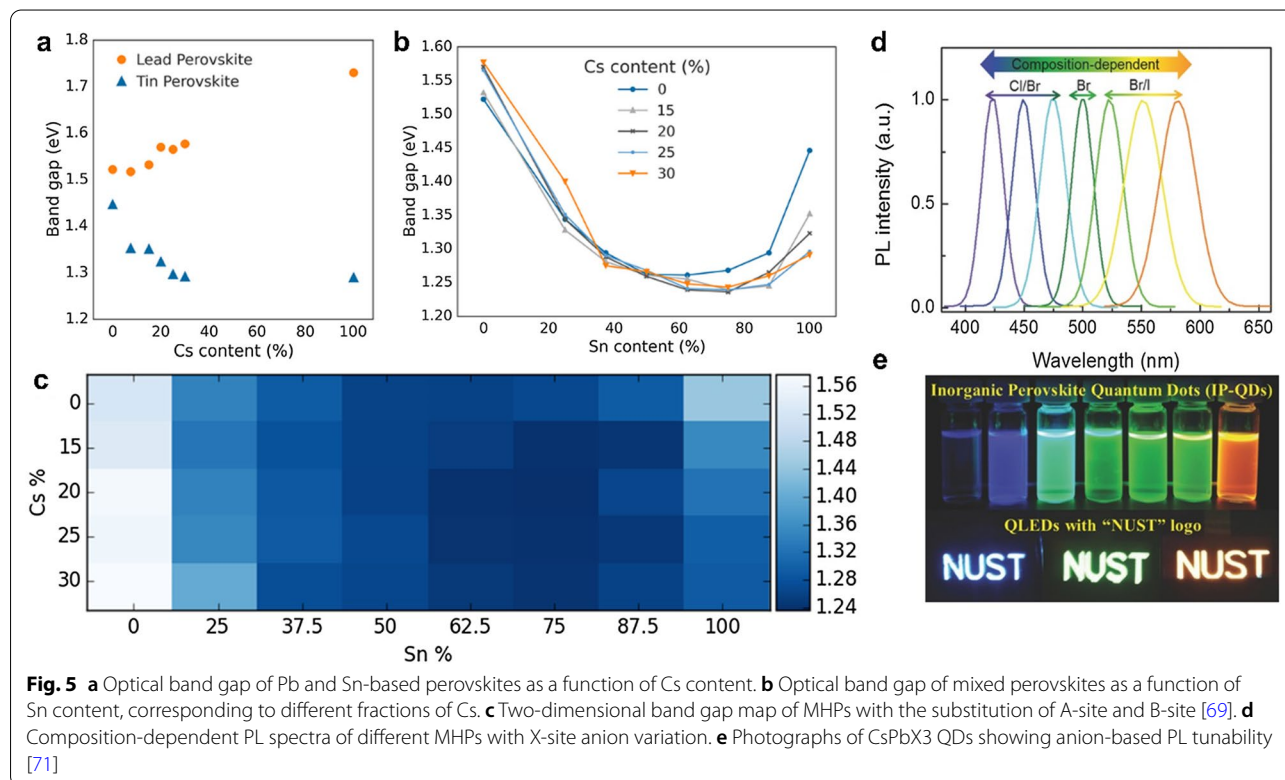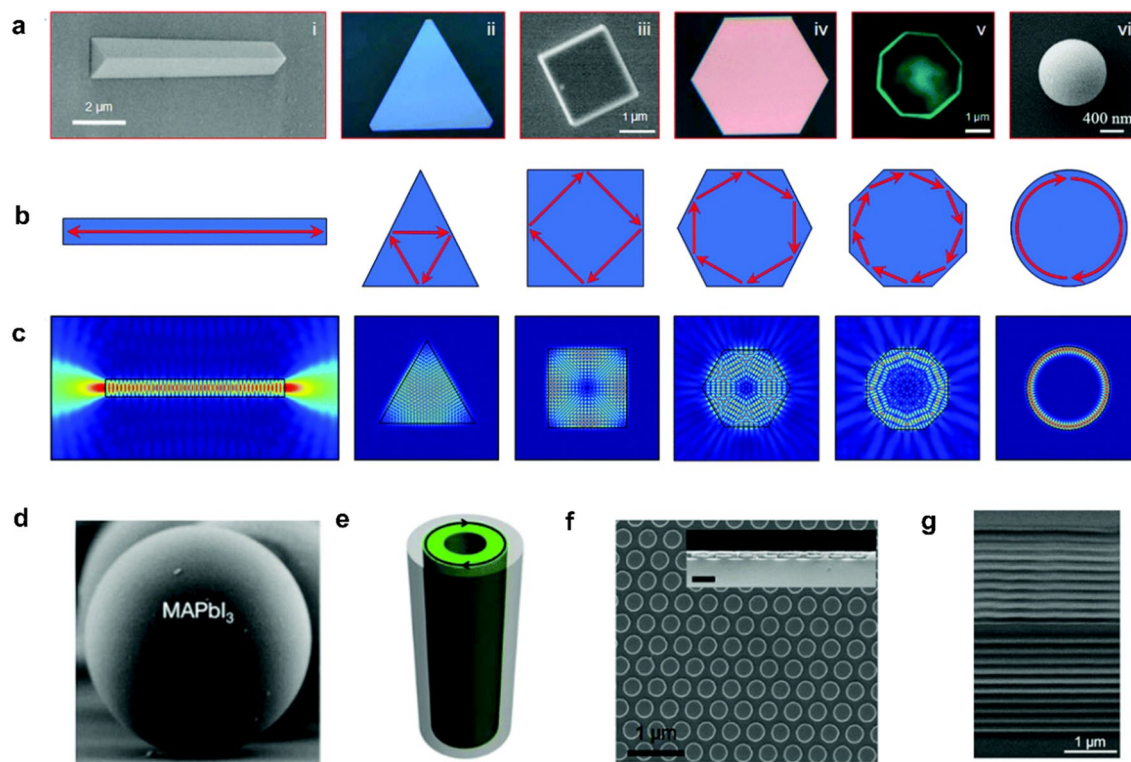
### 3.3 Composition
Benefiting from the ionic nature, MHPs family perform flexible chemical management via substitution of A, B and X site, which enables tunable optoelectronic properties, such as band gap, PL diversity, carrier transport, and so on. For example, it is obvious that $FAPbI_3$ shows the tunable band gap when using substitution of the A-site cation with Cs and B-site with Sn (Fig. 5a–c). The tunable optical band gaps achieved by compositional change provides a general framework of design rules for desired band gap and band positions of particular MHP [69]. Particularly, Originating from the highly soluble precursors could lead to anion exchange in a few seconds without deteriorating the initial structure or forming any remarkable lattice/surface defects, anion doping is widely used to tune the chemical composition and optical properties of more stable $CsPbX_3$ nanostructures [70], which has

enabled MHPs to be suitable for multiple applications, such as light-emitting diodes, wavelength-tunable lasers, and photodetectors that operation of wide spectral range. As shown in Fig. 5d and e, PL emission of $CsPbX_3$ QDs could be varied from UV to NIR spectral regions owing to the anion-based spectral tunability, leading to the QLED devices with the emission of uniform and large-area blue, green, and orange light [71].

### 3.4 Geometry
The optoelectronics of MHPs can also be readily modulated by changing the crystal geometry, especially in the MHP laser field, where lasing actions from different crystal geometry demonstrate different kinds of distinct microcavity effects. The key role of optical cavity is to provide optical feedback for laser oscillation, which defines the allowed cavity lasing modes within the gain spectrum as well as the spatial characteristics of the output beam [72]. There are mainly two kinds of optical microcavities for MHP lasers, including intrinsic and extrinsic cavities. The intrinsic cavity of MHPs is owing to the gain medium itself (*i.e.*, MHPs) with a particular geometric structure capable of providing the optical feedback. As shown in Fig. 6a, various geometries of MHPs micro/nanocrystals, including 1D nanowires, 2D triangular, tetragonal, hexagonal, and octagonal microdisks, and 3D microspheres, are

**Fig. 5** **a** Optical band gap of Pb and Sn-based perovskites as a function of Cs content. **b** Optical band gap of mixed perovskites as a function of Sn content, corresponding to different fractions of Cs. **c** Two-dimensional band gap map of MHPs with the substitution of A-site and B-site [69]. **d** Composition-dependent PL spectra of different MHPs with X-site anion variation. **e** Photographs of CsPbX3 QDs showing anion-based PL tunability [71]

**Fig. 6** **a**–**c** Intrinsic cavities of MHPs. **a** Perovskite crystals with different morphologies, including 1D (i) nanowires, 2D (ii) triangular, (iii) tetragonal, (iv) hexagonal, and (v) octagonal microdisks, and 3D (vi) microspheres. **b** Optical trajectories and **c** The corresponding simulated field distribution of perovskite cavities with different morphologies [72]. **d**–**g** Extrinsic cavities of MHPs, **d** side-view SEM image of a microsphere cavity [74]. **e** Schematic diagrams of capillary cavity with circular WGM laser resonances [75]. **f** SEM image of DFB laser on a quartz substrate [76]. **g** Cross-sectional SEM image of a perovskite DBR laser device [77]

obtained by different synthesis approaches [72], indicating a geometry-dependent microcavity effects. For example, the MAPbBr$_3$ perovskite 1D microwires with rectangular cross section shows Fabry-Pérot (FP) longitudinal cavity effects, while for the 2D microplates, exhibits a four-edge reflected whispering-gallery-mode (WGM) lasing action (Fig. 6b, c) [73]. While the extrinsic cavity of MHPs is realized by introducing an additional geometry that induces the optical feedback to MHPs, including microsphere and capillary cavities [74, 75], DFB cavity [76], and distributed Bragg reflector (DBR) cavity [77], as shown in Fig. 6d–g. MHPs as gain media can be integrated with the extrinsic cavities through various techniques, such as spin-coating, inkjet-print, vacuum thermal evaporation, and so on. Such merits of MHPs would help us to fabricate mini-sized lasers with specific functionalities through better understanding the structure–property relations, and to promote the advancement of metal hybrid flexible optical elements into mini-sized photonic circuits with higher performance [73].

## 4 Optoelectronic devices based on MHPs

Owing to the unique optoelectronic features of MHPs, they have been extensively investigated in various optoelectronic devices, where MHPs mainly serve as light harvest or a light emitter. The light harvesting devices, such as solar cells and photodetectors, convert incident photons into free charge carries in MHPs (red boxes in Fig. 7). Different from the typical sandwich architecture of solar cells, PDs can be classified into vertical and lateral structures. The vertical-structure PDs (*i. e.,* photodiodes) have the similar configuration to the photovoltaic device, while the lateral-structure PDs (*i. e.,* phototransistor and photoconductor), being known as photoconductive type, includes the metal–semiconductor-metal and the field-effect transistor configuration, showing the functions of light detection and signal amplification simultaneously. As for the light-emitting devices, a typical perovskite LED usually turns the injected charge carriers into luminescent layer under forward bias, where they recombine radiatively and emit light in all directions (green box in

**Fig. 7** The nature of photogenerated exciton/carriers within perovskites and the photophysical process in various optoelectronic devices [88]
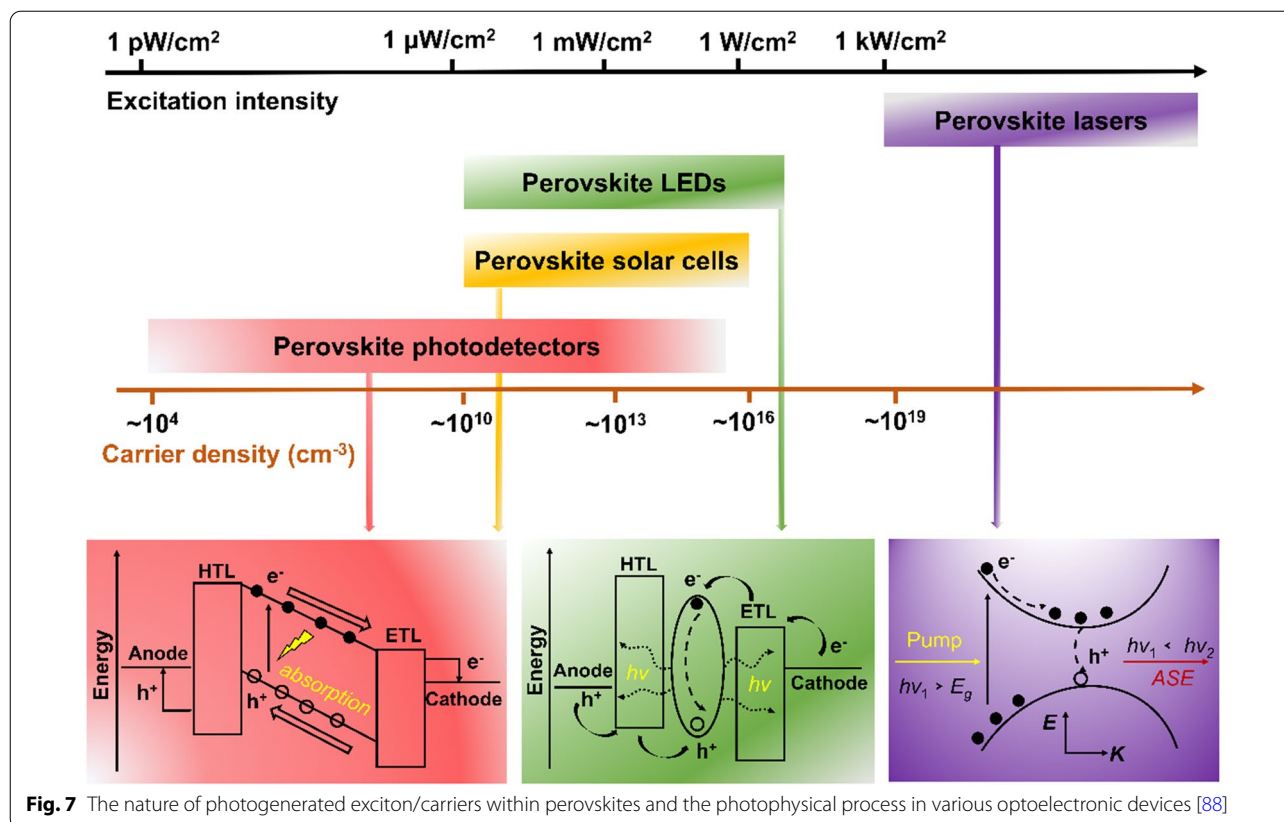
Fig. 7). While lasers essentially work based on a light-amplification process by stimulated emission of radiation (purple box in Fig. 7) [78, 79].

Management of light, such as emission, absorption, modulation and transmission, is the core of optoelectronic device and is principally governed by the photogenerated carrier behavior, and the optoelectronic devices correspond to various photophysical processes, which have their own suitable working conditions, including excitation density and carrier density [80]. As shown in Fig. 7, under low excitation fluence with carrier densities region from $\sim 10^4$ to $\sim 10^{17}$ cm$^{-3}$, the typical photovoltaic devices (*i.e.* PDs, PSCs and LEDs) are usually evaluated, where the PDs with detectable light intensities rang from 1pW cm$^2$ to $\sim 100$ mW/cm$^2$ [81, 82], PSCs with light intensities are over a range of $\sim 1$ μW/cm$^2$ to $\sim 1000$ mW/cm$^2$ [83, 84], and LEDs can further extend the working range of the device from $\sim 1$ μW/cm$^2$ to $\sim 10$ mW/cm$^2$ [85, 86]. As the excitation intensity reaches beyond 100 mW/cm$^2$, the effect of ASE behavior can even be realized along with the carrier density reaches over $\sim 10^{18}$ cm$^{-3}$ [10, 87], leading to the realization of optically pumped perovskite lasers.

## 5 Revolutionary applications of MHPs-based devices

Owing to the unique optoelectronic properties of MHPs, the application of MHPs-based optoelectronic devices in various fields has been widely investigated, including energy harvest/conversion, imaging/sensing, display/communication, and manufacture/medicine as shown in Fig. 8. In these applications, MHPs exhibit superior performance compared to the traditional materials, such as high efficiency, flexibility, tunability, and versatility. Taking advantages of these merits, MHPs are expected to make indispensable contribution to the advanced revolutionary technologies that could benefit the mankind, such as functional integration system, information display system, electronic communication system, and health & medical system. In this section, the advanced development of MHPs-based optoelectronic devices used in those systems will be briefly introduced.

### 5.1 Functional integration system

Inspired by the unique merits of MHPs, such as low cost, semi-transparent, high energy/mass ratio, and flexibility, MHPs as photo-electric unit have been explored to develop potential applications in the next-generation
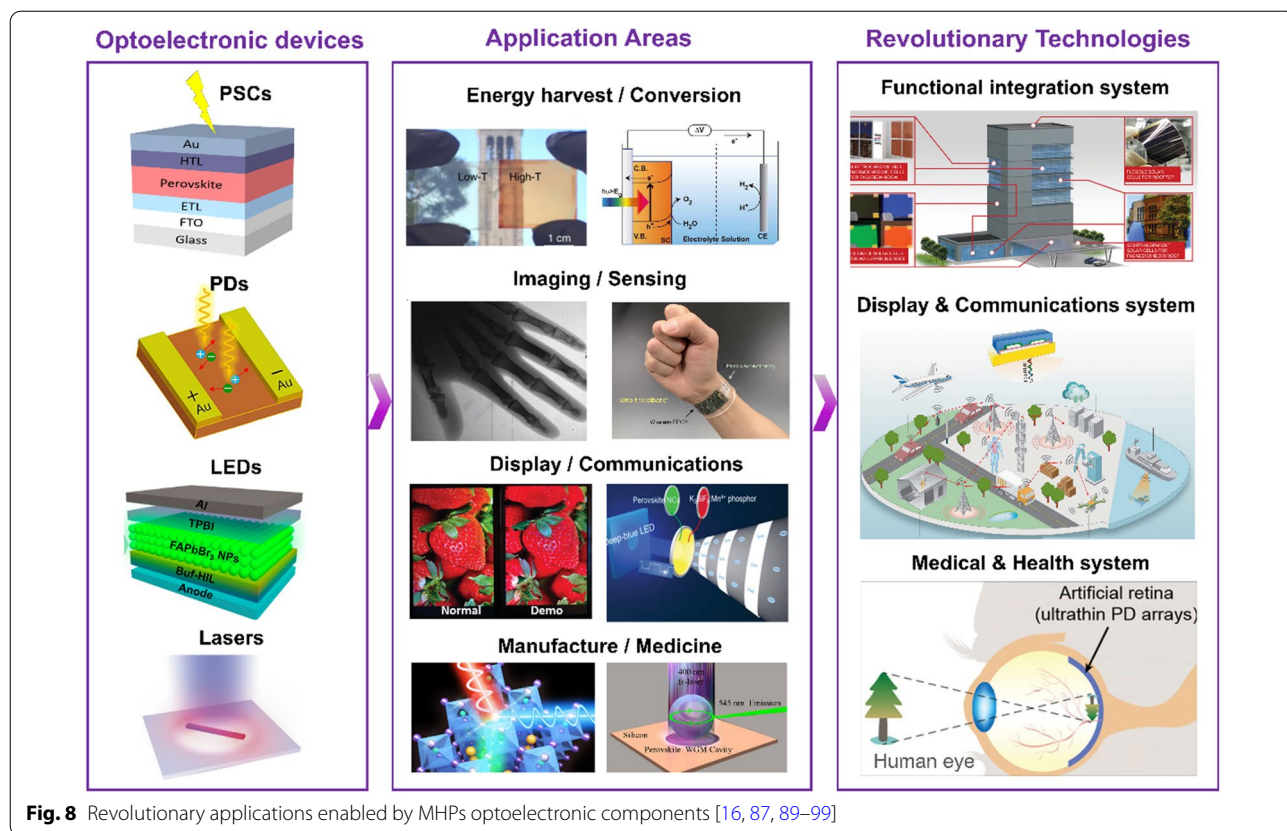
**Fig. 8** Revolutionary applications enabled by MHPs optoelectronic components [16, 87, 89–99]

functional integration system, including smart photovoltaic windows energy conversion & storage system, and self-powered system.

Integrated smart photovoltaic windows based on MHPs are regarded as highly an efficient and promising green technology, which have been praised for the broaden application, including BIPVs, self-powered electronic device displays, and solar-powered automobile roofs [91, 100]. Compared to traditional opaque solar cells, semitransparent perovskite solar cells (ST-PSCs), using phase transformative perovskites can switch between semitransparent and transparent states, demonstrating the potential in realizing the integration both functions composed of color-adjustment and power-generation, and solving the fundamental trade-off between transparency and solar energy harvesting of conventional semiconductor materials [101–103].

Next-generation internet of things (IoT), smart cities, and wearable electronics, are expected to be self-powered by conformable energy storage devices that can provide energy output whenever needed. Therefore, the integrated photoelectric conversion-storage systems, which can transfer the photo-generated electrons and holes from the excited perovskite and electrochemically store in the storage devices, has offered a promising solution.

Also, the system gained great scientific and technological attention due to the increasing demand for green energy and the tendency for miniaturization and multi-functionalization in photo-electronic industry. Since the concept of "photo-capacitor" was first proposed by Tsutomu Miyasaka in 2004 [104], efforts for integrated photoelectric conversion-storage systems have been made, ranging from PSCs-lithium ion batteries (LIBs), PSCs-supercapacitors (SCs), and PSCs with other types of energy storage devices [105, 106]. These integrated systems enable the development of flexible and self-powered electronics, which have attracted tremendous research interests due to their applications in wearable and portable devices. One of the critical issues needs to be addressed for integrated system is the inherent mismatch between low voltage, high current solar cells and high voltage, low current batteries. In this regard, it is challenging but of great significance to develop integrated systems with both high-power density and large energy density, leading to the high overall photoelectric conversion and storage efficiency of the integrated system.

In sum, the functional integration system based on MHPs photo-electric devices may become one of the most disruptive technologies for the smart cities, IoT, and wearable electronics.

## 5.2 Information display system

Next-generation display system require efficient light sources that combine high brightness, high color purity, high stability, compatibility with flexible substrates, and transparency. In order to meet these requirements, researchers have never stopped exploring and pursuing better display materials and technologies. Compared with the existing commercial phosphor, MHPs are shown to fulfill all the requirements above, which has been widely regarded as a promising candidate of next generation display system.

LEDs, which convert electricity to light, are widely used in modern society-for example, in lighting, flat-panel displays, medical devices and many other situations [107, 108]. Inspiringly, perovskite-based light-emitting diodes (PeLEDs) have become an ideal candidate for next-generation solid-state lightings and high-definition displays due to their high PLQY, tunable emission wavelength over the visible spectrum, and narrow emission. In recent years, prominent progress has been achieved for PeLEDs, whoes EQE has reached over 20% for green and red PeLEDs, while high-performing blue PeLEDs remains a big challenge [109, 110]. In addition to PeLEDs, the unique properties of MHPs enable them to potentially go beyond many other information display systems. For example, the excellent performance of PeLEDs and hybrid LEDs based on inorganic QDs and perovskites in the NIR region may bring about new applications in biomedical diagnosis and a variety of wearable electronic devices [111]. Moreover, the good mechanical property of MHPs promotes their application in stretchable electronics that are soft and elastic, which has been considered as the next generation of smart electronics with enhanced functionality, usability, and aesthetics. Notably, stretchable displays and solid-state lighting systems are emerging technologies factors that can conform to diverse applications, such as expandable and foldable screens for information technologies, bio-integrated devices, and wearable electronic clothing.

## 5.3 Electronic communication system

The continuing development of consumer electronics, mobile communications and advanced computing technologies has led to a rapid growth in data traffic, creating challenges for the communications industry. PeLEDs, which can offer tunable optoelectronics properties and solution-processable manufacturing, are of particular interest in the development of next-generation data communications [99]. In addition, photodetectors are key components of many electronic products, such as digital camera, smart phone, and medical diagnostics instrument, which are important for imaging and optical communication applications [112–114]. In the last decade, with the continuous rise of autonomous driving, environmental monitoring, optical communication, or biosensors, there is a more prominent demand for excellent photodetectors. Moreover, laser technology has become ubiquitous in every section of modern society, such as scientific research, manufacturing, communication and so on. The possibility of developing efficient on-chip coherent light sources from electrically pumped semiconductor laser diodes (LDs) has been the center of attention for researchers in the integrated optoelectronic field [115–117].

Owing to the advantages of MHPs material, it could play a key role in the next-generation electronic communication system, and MHPs-based LEDs, PDs, and LDs can be applied in widespread communication solutions in future scenarios. For instance, integrated components for short-range communications with rigorous latency requirements (for example, self-guiding vehicles), flexible biosensors (for example, real-time health monitoring and disposable lab-on-a-chip for point-of-care diagnostics), light communication, underwater communications, low-cost on-chip IoT sensors for accurate tracking and positioning, indoor data services (for example, Li-Fi and short-distance on-board communications).

## 5.4 Health & medical system

Among the various optoelectronic applications, MHPs have also attracted significant interest in health & medical systems such as health monitoring, biomedicine, medical imaging techniques. The use of digital flat detectors in many diagnostic and interventional medical applications, including in X-ray imaging procedures, has increased rapidly over the past decades [112]. For example, medical X-ray imaging procedures require digital flat detectors operating at low doses to reduce radiation health risks, while solution processed organic–inorganic hybrid perovskites have characteristics that make them good candidates for the photoconductive layer of such sensitive detectors [16, 21]. Recent researches on the X-ray scintillator (*i. e.*, all-inorganic perovskite nanocrystals $CsPbBr_3$ QDs) have shown that the color-tunable perovskite nanocrystal scintillators can provide a facile visualization way for X-ray radiography [21]. In addition, perovskites integrated with chiral ligands exhibits superior chiroptoelectronic property in recent years, and circularly polarized photodetectors and light sources based on these materials are promising for flexible integrated devices [118]. However, to promote the commercialization, MHPs-based devices will face many of the same challenges that PSCs face, specifically, stability, toxicity issues, and competition from more mature competing technologies.

# 6 Challenges and perspectives of MHPs

## 6.1 Instability

Despite impressive advances of MHPs, their typical challenges, such as long-term instability and toxicity, greatly impede their rapid commercialization (Fig. 9). The instability problem is origin from the structural degradation under certain conditions, which includes intrinsic and extrinsic sources. The initial intrinsic stability of MHP can be primarily evaluated by the Goldschmidt tolerance factor ($\tau$), which is an empirical index widely applied to the evaluation of the geometry stability of perovskite crystal, and the value of $\tau$ in the range of 0.8–1 favored an ideal cubic perovskite structure [119]. However, for MHPs with $\tau$ value out of the 0.8–1 range (*e.g.*, $FAPbI_3 > 1$), formation of secondary non-perovskite phases ($\delta$-$FAPbI_3$) can also influence the device performance and stability [120]. Introduction of MA cation or Cs cation has been the most common strategy to enable the stabilization of black-phase $FAPbI_3$ perovskite, but the resulted mixed cation perovskite may broaden the optical bandgap and possibly inducing the inferior thermal stability. Moreover, intrinsic ion migration in MHPs has also been shown to occur under the drive of electric filed, resulting in the abnormal *J-V* hysteresis, phase segregation, slow photoconductivity response, and device performance degradation [24]. In addition, characteristics of polycrystalline films can also be intrinsic sources of instability too, for instance, high density of grain boundaries and thermal strain generated during the annealing process of perovskite films accelerates degradation of the perovskite. Therefore, how to stabilize black-phase $FAPbI_3$ to prepare high-stability and high-purity film is still the primary problem that needs to overcome to achieve efficient and stable PSCs [121]. Some volatile additives, such as FAAc, have been recently introduced to form the intermediate phase, facilitating the formation of stable $\alpha$-$FAPbI_3$ [122]. In addition, a mechanochemical strategy to prepare high quality $\alpha$-$FAPbI_3$ was demonstrated by Zhu and co-workers, where they prepare the $\delta$-$FAPbI_3$ perovskite powder first, and redissolving it in precursor solution, leading to a high concentration of large-sized polyiodide colloids and further enabling the formation of black-phase $FAPbI_3$. As a result, the devices deliver a champion PCE of 24.22% [123].

In addition to the intrinsic stability of perovskites, external environments, such as moisture, oxygen, heat, light, external bias, and contact layers, are also shown to be the origin of the instability problem of MHP-based devices. Instability against moisture and $O_2$ can be completely solved by standard encapsulation of the device, while the instability induced by light, external bias and contact layers are unavoidable in a working device and should be seriously handled [124]. Ion migration, trap state generation, etc. have been found to be reasons for performance deterioration under these external factors, and some of the most impressive strategies have been reported by 2D/3D heterojunction, defect passivation, interfacial stabilization, structural healing, strain release and device encapsulation [125–128], pushing the rapid development of the long-term stability of MHPs.

## 6.2 Toxicity

Apart from long term stability, toxicity of perovskite materials for both humans and ecosystem is an
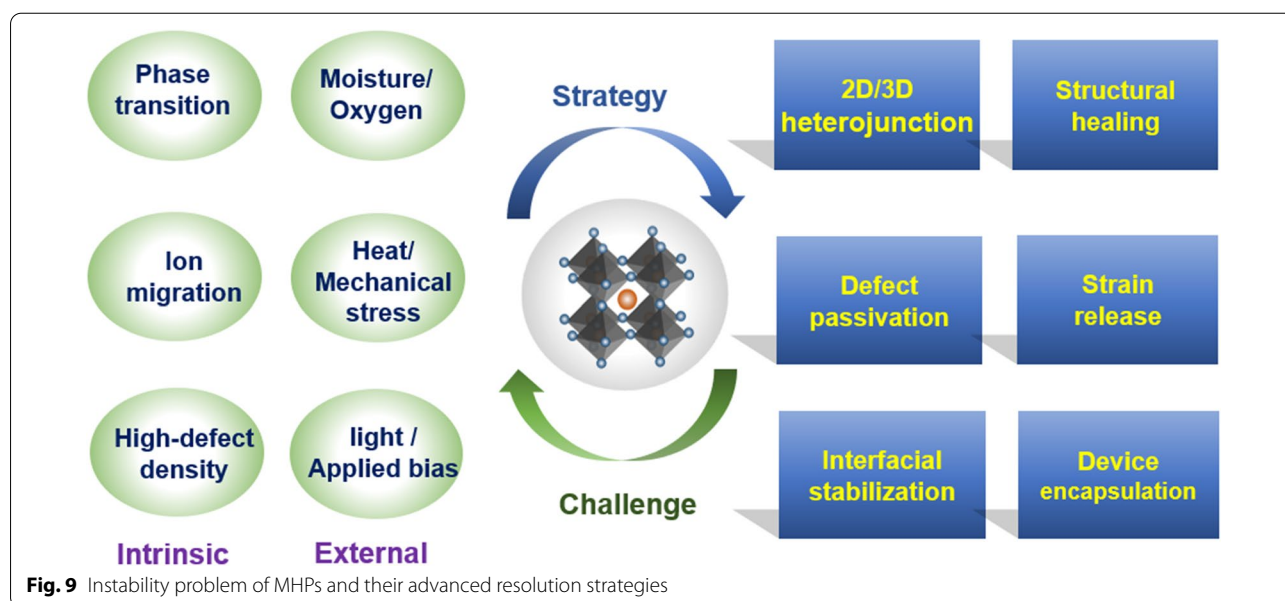


**Fig. 9** Instability problem of MHPs and their advanced resolution strategies

**Fig. 10** Toxicity problem of MHPs and their advanced resolution strategies [129]
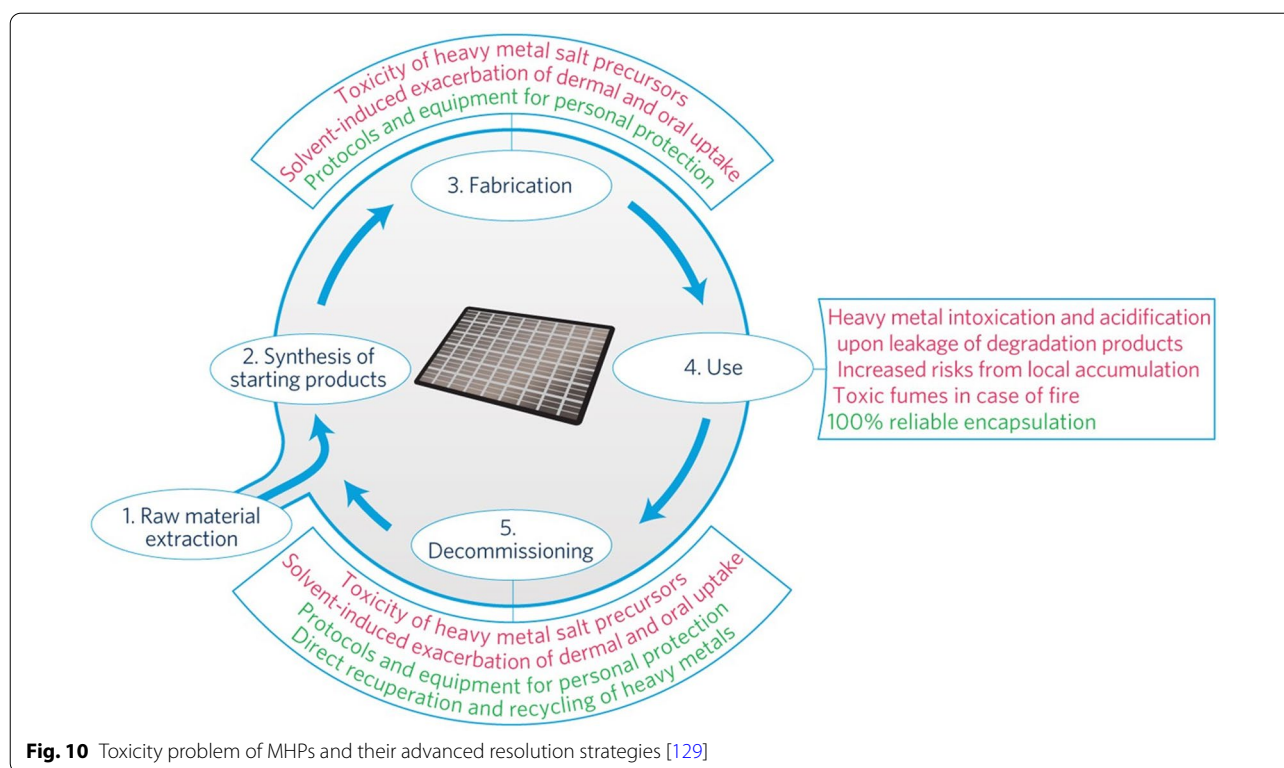
overwhelming challenge, which may hinder the commercialization pace of MHPs-based optoelectronic devices. As shown in Fig. 10, the life cycle of MHPs typically undergoes from raw material extraction, synthesis, film fabrication to the usage and finally decommissioning stage [129]. Strategies of preventing the lead leakage, such as physical encapsulation (*e. g.*, inserting the epoxy resin into the device module and the top glass cover), chemical absorption (e. g., introducing metal–organic framework as scaffolds) [130], eco-friendly perovskite materials (*e. g.*, $Sn^{2+}$, $Sb^{2+}$, $Ge^{2+}$, $Cu^{2+}$ and mixed monovalent and trivalent elements for double-perovskite structures) [131], and recycling strategy have been developed. Future research on the safe deployment of MHPs optoelectronic technology relies entirely on adopting precautionary measures against contamination at each stage of the device's life, from fabrication to disposal/recycling, and test standards should be also established.

## 7 Conclusions
As the rising star in the field of optoelectronics, MHPs with extraordinary properties have experienced unprecedented rapid development during the past decades. Here, we give an overview on the prominent optoelectronic properties of MHPs and their revolutionary applications in advanced technologies, which might greatly change the development course of human society. Nevertheless, to promote the large-scale utilization of MHPs, there are still many technique problems to be overcome, and vast investments are required to establish the building of MHPs-based optoelectronics. Overall, one can expect that in the next decade, MHPs will be under the spotlight in the era of "light".

**Author contributions**
HD, CR, and WG mainly wrote the manuscript and produced the figures. MJ, XY, and WH gave the advices and involved in revising the manuscript. All the authors participated in the discussion and confirmed the final version of the manuscript. CR, XY and WH guided all aspects of the work. All authors read and approved the final manuscript.

**Availability of data and materials**
Not applicable.

## Declarations

### Author details
[1]Frontiers Science Center for Flexible Electronics, Xi'an Institute of Flexible Electronics (IFE) and Xi'an Institute of Biomedical Materials & Engineering, Northwestern Polytechnical University, Xi'an 710072, China. [2]Key Laboratory of Flexible Electronics (KLOFE) & Institution of Advanced Materials (IAM), Nanjing Tech University (NanjingTech), Nanjing 211816, Jiangsu, China. [3]Key Laboratory for Organic Electronics & Information Displays (KLOEID), and Institute of Advanced Materials (IAM), Nanjing University of Posts and Telecommunications, Nanjing 210023, Jiangsu, China. [4]Department of Applied Physics, The Hong Kong Polytechnic University, Kowloon 999077, Hong Kong, China. [5]Shenzhen Research Institute, The Hong Kong Polytechnic University, Shenzhen 518057, Guangdong, China.

### References
1. C.K. Moller, Crystal structure and photoconductivity of caesium plumbohalides. Nature **182**, 1436–1436 (1958)
2. D.B. Mitzi, C.A. Feild, W.T.A. Harrison, A.M. Guloy, Conducting tin halides with a layered organic-based perovskite structure. Nature **369**, 467–469 (1994)
3. H.J. Snaith, Perovskites: the emergence of a new era for low-cost, high-efficiency solar cells. J. Phys. Chem. Lett. **4**, 3623–3630 (2013)
4. K. Tanaka et al., Electronic and excitonic structures of inorganic–organic perovskite-type quantum-well crystal ($C_4H_9NH_3)_2PbBr$ 4. Jpn. J. Appl. Phys. **44**, 5923–5932 (2005)
5. J.S. Manser, J.A. Christians, P.V. Kamat, Intriguing optoelectronic properties of metal halide perovskites. Chem. Rev. **116**, 12956–13008 (2016)
6. T.A. Takashi Kondo, T.Y. Ryoichilto, Biexciton lasing in the layered perovskite-type material ($C_6H_{13}NH_3)2PbI4$. Solid State Commun. **105**, 253–255 (1998)
7. A. Kojima, K. Teshima, Y. Shirai, T. Miyasaka, Organometal halide perovskites as visible-light sensitizers for photovoltaic cells. J. Am. Chem. Soc. **131**, 6050–6051 (2009)
8. Editorial, Perovskite fever. Nat. Mater. **13**, 837 (2014)
9. H. Dong et al., Crystallization dynamics of sn-based perovskite thin films: toward efficient and stable photovoltaic devices. Adv. Energy Mater. **12**, 2102213 (2021)
10. G. Xing et al., Low-temperature solution-processed wavelength-tunable perovskites for lasing. Nat. Mater. **13**, 476–480 (2014)
11. Q. Zhang, S.T. Ha, X. Liu, T.C. Sum, Q. Xiong, Room-temperature near-infrared high-Q perovskite whispering-gallery planar nanolasers. Nano Lett. **14**, 5995–6001 (2014)
12. F. Deschler et al., High photoluminescence efficiency and optically pumped lasing in solution-processed mixed halide perovskite semiconductors. J. Phys. Chem. Lett. **5**, 1421–1426 (2014)
13. S. Yakunin et al., Low-threshold amplified spontaneous emission and lasing from colloidal nanocrystals of caesium lead halide perovskites. Nat. Commun. **6**, 8056 (2015)
14. Z.-K. Tan et al., Bright light-emitting diodes based on organometal halide perovskite. Nat. Nanotechnol. **9**, 687–692 (2014)
15. S. Yakunin et al., Detection of X-ray photons by solution-processed organic-inorganic perovskites. Nat. Photon. **9**, 444–449 (2015)
16. Y.C. Kim et al., Printable organometallic perovskite enables large-area, low-dose X-ray imaging. Nature **550**, 87–91 (2017)
17. X. Qi et al., Photonics and optoelectronics of 2D metal-halide perovskites. Small **14**, 1800682 (2018)
18. K. Lin et al., Perovskite light-emitting diodes with external quantum efficiency exceeding 20 per cent. Nature **562**, 245–248 (2018)
19. T. Chiba et al., Anion-exchange red perovskite quantum dots with ammonium iodine salts for highly efficient light-emitting devices. Nat. Photon. **12**, 681–687 (2018)
20. W. Xu et al., Rational molecular passivation for high-performance perovskite light-emitting diodes. Nat. Photon. **13**, 418–424 (2019)
21. Q. Chen et al., All-inorganic perovskite nanocrystal scintillators. Nature **561**, 88–93 (2018)
22. Best research-cell efficiencies: http://www.Nrel.Gov (accessed: June 2022).
23. K. Chen, S. Schunemann, S. Song, H. Tuysuz, Structural effects on optoelectronic properties of halide perovskites. Chem. Soc. Rev. **47**, 7045–7077 (2018)
24. A.K. Jena, A. Kulkarni, T. Miyasaka, Halide perovskite photovoltaics: background, status, and future prospects. Chem. Rev. **119**, 3036–3103 (2019)
25. L.M. Herz, Charge-carrier mobilities in metal halide perovskites: fundamental mechanisms and limits. ACs Energy Lett. **2**, 1539–1548 (2017)
26. Y. Wang, Y. Zhang, P. Zhang, W. Zhang, High intrinsic carrier mobility and photon absorption in the perovskite $CH_3NH_3PbI_3$. Phys. Chem. Chem. Phys. **17**, 11516–11520 (2015)
27. G.W. Kim, A. Petrozza, Defect tolerance and intolerance in metal-halide perovskites. Adv. Energy Mater. **10**, 2001959 (2020)
28. G.W.P. Adhyaksa et al., Carrier diffusion lengths in hybrid perovskites: processing, composition, aging, and surface passivation effects. Chem. Mater. **28**, 5259–5263 (2016)
29. Y.-C. Hsiao et al., Fundamental physics behind high-efficiency organometal halide perovskite solar cells. J. Mater. Chem. A **3**, 15372–15385 (2015)
30. C.C. Stoumpos, M.G. Kanatzidis, The renaissance of halide perovskites and their evolution as emerging semiconductors. Acc. Chem. Res. **48**, 2791–2802 (2015)
31. D.B. Mitzi, Introduction: perovskites. Chem. Rev. **119**, 3033–3035 (2019)
32. A. Marronnier et al., Anharmonicity and disorder in the black phases of cesium lead iodide used for stable inorganic perovskite solar cells. ACS Nano **12**, 3477–3486 (2018)
33. S. Liu et al., Manipulating efficient light emission in two-dimensional perovskite crystals by pressure-induced anisotropic deformation. Sci. Adv. **5**, eaav9445 (2019)
34. F. Palazon et al., Changing the dimensionality of cesium lead bromide nanocrystals by reversible postsynthesis transformations with amines. Chem. Mater. **29**, 4167–4171 (2017)
35. C.C. Stoumpos, C.D. Malliakas, M.G. Kanatzidis, Semiconducting tin and lead iodide perovskites with organic cations: phase transitions, high mobilities, and near-infrared photoluminescent properties. Inorg. Chem. **52**, 9019–9038 (2013)
36. A.A. Zhumekenov et al., Formamidinium lead halide perovskite crystals with unprecedented long carrier dynamics and diffusion length. ACS Energy Lett. **1**, 32–37 (2016)
37. Q. Han et al., Single crystal formamidinium lead iodide ($FAPbI_3$): insight into the structural, optical, and electrical properties. Adv. Mater. **28**, 2253–2258 (2016)
38. M.C. Gelvez-Rueda, N. Renaud, F.C. Grozema, Temperature dependent charge carrier dynamics in formamidinium lead iodide perovskite. J. Phys. Chem. C **121**, 23392–23397 (2017)
39. G.A. Elbaz et al., Unbalanced hole and electron diffusion in lead bromide perovskites. Nano Lett. **17**, 1727–1732 (2017)
40. L. Wang, K. Wang, B. Zou, Pressure-induced structural and optical properties of organometal halide perovskite-based formamidinium lead bromide. J. Phys. Chem. Lett. **7**, 2556–2562 (2016)
41. S.D. Stranks et al., Electron-hole diffusion lengths exceeding 1 micrometer in an organometal trihalide perovskite absorber. Science **342**, 341–344 (2013)
42. A. Poglitsch, D. Weber, Dynamic disorder in methylammoniumtrihalogenoplumbates (ii) observed by millimeter-wave spectroscopy. J. Chem. Phy. **87**, 6373–6378 (1987)
43. D. Shi et al., Solar cells. Low trap-state density and long carrier diffusion in organolead trihalide perovskite single crystals. Science **347**, 519–522 (2015)
44. A. Jaffe et al., High-pressure single-crystal structures of 3D lead-halide hybrid perovskites and pressure effects on their electronic and optical properties. ACS Cent. Sci. **2**, 201–209 (2016)

45. G. Maculan et al., $CH_3NH_3PbCl_3$ single crystals: Inverse temperature crystallization and visible-blind UV-photodetector. J. Phys. Chem. Lett. **6**, 3781–3786 (2015)

46. W. Peng et al., Solution-grown monocrystalline hybrid perovskite films for hole-transporter-free solar cells. Adv. Mater. **28**, 3383–3390 (2016)

47. C.C. Stoumpos et al., Crystal growth of the perovskite semiconductor $CsPbBr_3$: a new material for high-energy radiation detection. Cryst. Growth Des. **13**, 2722–2727 (2013)

48. B. Yang et al., Ultrasensitive and fast all-inorganic perovskite-based photodetector via fast carrier diffusion. Adv. Mater. **29**, 1703758 (2017)

49. F. Chen et al., Crystal structure and electron transition underlying photoluminescence of methylammonium lead bromide perovskites. J. Mater. Chem. C **5**, 7739–7745 (2017)

50. M. Sebastian et al., Excitonic emissions and above-band-gap luminescence in the single-crystal perovskite semiconductors $CsPbBr_3$ and $CsPbCl_3$. Phys. Rev. B **92**, 235210 (2015)

51. S.Y.J.A.R. Lima, Ferroelastic phase transition and twin structure by $^{133}Cs$ NMR in a cspbcl$_3$ single crystal. Phys. B **304**, 79–85 (2001)

52. Y. Rakita et al., Low-temperature solution-grown $CsPbBr_3$ single crystals and their characterization. Crys. Growth Des. **16**, 5717–5725 (2016)

53. M.I. Saidaminov et al., Perovskite photodetectors operating in both narrowband and broadband regimes. Adv. Mater. **28**, 8144–8149 (2016)

54. Y. Liu et al., 20-mm-large single-crystalline formamidinium-perovskite wafer for mass production of integrated photodetectors. Adv. Opt. Mater. **4**, 1829–1837 (2016)

55. L. Gu et al., 3D arrays of 1024-pixel image sensors based on lead halide perovskite nanowires. Adv. Mater. **28**, 9713–9721 (2016)

56. W. Deng et al., Aligned single-crystalline perovskite microwire arrays for high-performance flexible image sensors with long-term stability. Adv. Mater. **28**, 2201–2208 (2016)

57. D.H. Kang et al., An ultrahigh-performance photodetector based on a perovskite-transition-metal-dichalcogenide hybrid structure. Adv. Mater. **28**, 7799–7806 (2016)

58. D. Yang, D. Ma, 1,1-bis[(di-4-tolylamino)phenyl]cyclohexane for fast response organic photodetectors with high external efficiency and low leakage current. J. Mater. Chem. C **1**, 2054–2060 (2013)

59. Z. Su et al., High-performance organic small-molecule panchromatic photodetectors. ACS Appl. Mater. Interfaces **7**, 2529–2534 (2015)

60. M.S. Jang, S. Yoon, K.M. Sim, J. Cho, D.S. Chung, Spatial confinement of the optical sensitizer to realize a thin film organic photodetector with high detectivity and thermal stability. J. Phys. Chem. Lett. **9**, 8–12 (2018)

61. S. Yoon, C.W. Koh, H.Y. Woo, D.S. Chung, Systematic optical design of constituting layers to realize high-performance red-selective thin-film organic photodiodes. Adv. Opt. Mater. **6**, 1701085 (2018)

62. G. Konstantatos et al., Ultrasensitive solution-cast quantum dot photodetectors. Nature **442**, 180–183 (2006)

63. G. Konstantatos et al., Hybrid graphene-quantum dot phototransistors with ultrahigh gain. Nat. Nanotechnol. **7**, 363–368 (2012)

64. G. Wang et al., Advances of nonlinear photonics in low-dimensional halide perovskites. Small **17**, 2100809 (2021)

65. M. Yuan et al., Perovskite energy funnels for efficient light-emitting diodes. Nat. Nanotechnol. **11**, 872–877 (2016)

66. L. Zhang et al., High-performance quasi-2D perovskite light-emitting diodes: From materials to devices. Light. Sci. Appl. **10**, 61 (2021)

67. L.N. Quan, F.P. Garcia de Arquer, R.P. Sabatini, E.H. Sargent, Perovskites for light emission. Adv. Mater. **30**, 1801996 (2018)

68. Y.P. Fu et al., Metal halide perovskite nanostructures for optoelectronic applications and the study of physical properties. Nat. Rev. Mater. **4**, 169–188 (2019)

69. R. Prasanna et al., Band gap tuning via lattice contraction and octahedral tilting in perovskite materials for photovoltaics. J. Am. Chem. Soc. **139**, 11117–11124 (2017)

70. Q.A. Akkerman et al., Tuning the optical properties of cesium lead halide perovskite nanocrystals by anion exchange reactions. J. Am. Chem. Soc. **137**, 10276–10281 (2015)

71. J. Song et al., Quantum dot light-emitting diodes based on inorganic perovskite cesium lead halides (cspbx$_3$). Adv. Mater. **27**, 7162–7167 (2015)

72. H. Dong, C. Zhang, X. Liu, J. Yao, Y.S. Zhao, Materials chemistry and engineering in metal halide perovskite lasers. Chem. Soc. Rev. **49**, 951–982 (2020)

73. W. Zhang et al., Controlling the cavity structures of two-photon-pumped perovskite microlasers. Adv. Mater. **28**, 4040–4046 (2016)

74. B.R. Sutherland, S. Hoogland, M.M. Adachi, C.T. Wong, E.H. Sargent, Conformal organohalide perovskites enable lasing on spherical resonators. ACS Nano **8**, 10947–10952 (2014)

75. Y. Wang et al., All-inorganic colloidal perovskite quantum dots: a new class of lasing materials with favorable characteristics. Adv. Mater. **27**, 7101–7108 (2015)

76. S. Chen et al., A photonic crystal laser from solution based organo-lead iodide perovskite thin films. ACS Nano **10**, 3959–3967 (2016)

77. S. Chen, A. Nurmikko, Stable green perovskite vertical-cavity surface-emitting lasers on rigid and flexible substrates. ACS Photon. **4**, 2486–2494 (2017)

78. T. Jeon et al., Hybrid perovskites: effective crystal growth for optoelectronic applications. Adv. Energy Mater. **7**, 1602596 (2017)

79. B.R. Sutherland, E.H. Sargent, Perovskite photonic sources. Nat. Photon. **10**, 295–302 (2016)

80. T.C. Sum et al., Spectral features and charge dynamics of lead halide perovskites: origins and interpretations. Acc. Chem. Res. **49**, 294–302 (2016)

81. Y. Fang, J. Huang, Resolving weak light of sub-picowatt per square centimeter by hybrid perovskite photodetectors enabled by noise reduction. Adv. Mater. **27**, 2804–2810 (2015)

82. S.-F. Leung et al., A self-powered and flexible organometallic halide perovskite photodetector with very high detectivity. Adv. Mater. **30**, 1704611 (2018)

83. Q. Lin, Z. Wang, H.J. Snaith, M.B. Johnston, L.M. Herz, Hybrid perovskites: prospects for concentrator solar cells. Adv. Sci. **5**, 1700792 (2018)

84. N. Marinova et al., Light harvesting and charge recombination in $CH_3NH_3PbI_3$ perovskite solar cells studied by hole transport layer thickness variation. ACS Nano **9**, 4200–4209 (2015)

85. C. Zou, Y. Liu, D.S. Ginger, L.Y. Lin, Suppressing efficiency roll-off at high current densities for ultra-bright green perovskite light-emitting diodes. ACS Nano **14**, 6076–6086 (2020)

86. N. Wang et al., Perovskite light-emitting diodes based on solution-processed self-organized multiple quantum wells. Nat. Photon. **10**, 699–704 (2016)

87. H. Zhu et al., Lead halide perovskite nanowire lasers with low lasing thresholds and high quality factors. Nat. Mater. **14**, 636–642 (2015)

88. J. Qin, X.-K. Liu, C. Yin, F. Gao, Carrier dynamics and evaluation of lasing actions in halide perovskites. Trends Chem. **3**, 34–46 (2021)

89. Y. Shen et al., Centimeter-sized single crystal of two-dimensional halide perovskites incorporating straight-chain symmetric diammonium ion for x-ray detection. Angew. Chem. Int. Ed. **59**, 14896–14902 (2020)

90. Y.-H. Kim et al., High efficiency perovskite light-emitting diodes of ligand-engineered colloidal formamidinium lead bromide nanoparticles. Nano Energy **38**, 51–58 (2017)

91. J. Lin et al., Thermochromic halide perovskite solar cells. Nat. Mater. **17**, 261–267 (2018)

92. A. Guerrero, J. Bisquert, Perovskite semiconductors for photoelectrochemical water splitting applications. Curr. Opin. Electrochem **2**, 144–147 (2017)

93. X. Li et al., Facile in situ fabrication of cs$_4$pbbr$_6$ /cspbbr$_3$ nanocomposite containing polymer films for ultrawide color gamut displays. Adv. Opt. Mater. **8**, 2000232 (2020)

94. W. Deng et al., 2D ruddlesden–popper perovskite nanoplate based deep-blue light-emitting diodes for light communication. Adv. Funct. Mater. **29**, 1903861 (2019)

95. Q. Zhang, Q. Shang, R. Su, T.T.H. Do, Q. Xiong, Halide perovskite semiconductor lasers: materials, cavity design, and low threshold. Nano Lett. **21**, 1903–1914 (2021)

96. B. Tang et al., Single-mode lasers based on cesium lead halide perovskite submicron spheres. ACS Nano **11**, 10681–10688 (2017)

97. L. Shen, H.-L. Yip, F. Gao, L. Ding, Semitransparent perovskite solar cells for smart windows. Sci. Bull. **65**, 980–982 (2020)

98. W. Wu et al., Ultrathin and conformable lead halide perovskite photodetector arrays for potential application in retina-like vision sensing. Adv. Mater. **33**, 2006006 (2021)

99. A. Ren et al., Emerging light-emitting diodes for next-generation data communications. Nat. Electron. **4**, 559–572 (2021)

100. J. Bing et al., Perovskite solar cells for building integrated photovoltaics-glazing applications. Joule **6**, 1–29 (2022)
101. M. Batmunkh, Y.L. Zhong, H. Zhao, Recent advances in perovskite-based building-integrated photovoltaics. Adv. Mater. **32**, 2000631 (2020)
102. C. Roldán-Carmona et al., High efficiency single-junction semitransparent perovskite solar cells. Energy Environ. Sci. **7**, 2968–2973 (2014)
103. M. De Bastiani et al., Thermochromic perovskite inks for reversible smart window applications. Chem. Mater. **29**, 3367–3370 (2017)
104. T. Miyasaka, T.N. Murakami, The photocapacitor: an efficient self-charging capacitor for direct storage of solar energy. Appl. Phys. Lett. **85**, 3932–3934 (2004)
105. A. Gurung et al., Highly efficient perovskite solar cell photocharging of lithium ion battery using dc-dc booster. Adv. Energy Mater. **7**, 1602105 (2017)
106. C. Li et al., Wearable energy-smart ribbons for synchronous energy harvest and storage. Nat. Commun. **7**, 13319 (2016)
107. C. Zou, C. Chang, D. Sun, K.F. Böhringer, L.Y. Lin, Photolithographic patterning of perovskite thin films for multicolor display applications. Nano Lett. **20**, 3710–3717 (2020)
108. Y. Yin et al., Full-color micro-led display with cspbbr$_3$ perovskite and CdSe quantum dots as color conversion layers. Adv. Mater. Technol. **5**, 2000251 (2020)
109. Y. Cao et al., Perovskite light-emitting diodes based on spontaneously formed submicrometre-scale structures. Nature **562**, 249–253 (2018)
110. C. Ge, Q. Fang, H. Lin, H. Hu, Review on blue perovskite light-emitting diodes: recent advances and future prospects. Front. Mater. **8**, 635025 (2021)
111. Y.F. Li et al., Stretchable organometal-halide-perovskite quantum-dot light-emitting diodes. Adv. Mater. **31**, 1807516 (2019)
112. X. Ou et al., High-resolution x-ray luminescence extension imaging. Nature **590**, 410–415 (2021)
113. H. Wang, D.H. Kim, Perovskite-based photodetectors: materials and devices. Chem. Soc. Rev. **46**, 5204–5236 (2017)
114. W. Tian, L. Min, F. Cao, L. Li, Nested inverse opal perovskite toward superior flexible and self-powered photodetection performance. Adv. Mater. **32**, 1906974 (2020)
115. C. Cho et al., Electrical pumping of perovskite diodes: toward stimulated emission. Adv. Sci. **8**, 2101663 (2021)
116. A.P. Schlaus, M.S. Spencer, X.Y. Zhu, Light-matter interaction and lasing in lead halide perovskites. Acc. Chem. Res. **52**, 2950–2959 (2019)
117. Y.-S. Park, J. Roh, B.T. Diroll, R.D. Schaller, V.I. Klimov, Colloidal quantum dot lasers. Nat. Rev. Mater. **6**, 382–401 (2021)
118. G. Long et al., Chiral-perovskite optoelectronics. Nat. Rev. Mater. **5**, 423–439 (2020)
119. G. Kieslich, S. Sun, A.K. Cheetham, Solid-state principles applied to organic–inorganic perovskites: new tricks for an old dog. Chem. Sci. **5**, 4712–4715 (2014)
120. J.P. Correa-Baena et al., Promises and challenges of perovskite solar cells. Science **358**, 739–744 (2017)
121. T. Niu, L. Chao, X. Dong, L. Fu, Y. Chen, Phase-pure α-FAPbI$_3$ for perovskite solar cells. J. Phys. Chem. Lett. **13**, 1845–1854 (2022)
122. X. Ling et al., Combined precursor engineering and grain anchoring leading to ma-free, phase-pure, and stable alpha-formamidinium lead iodide perovskites for efficient solar cells. Angew. Chem. Int. Ed. **60**, 27299–27306 (2021)
123. Y. Zhang et al., Mechanochemistry advances high-performance perovskite solar cells. Adv. Mater. **34**, 2107420 (2022)
124. C.C. Boyd, R. Cheacharoen, T. Leijtens, M.D. McGehee, Understanding degradation mechanisms and improving stability of perovskite photovoltaics. Chem. Rev. **119**, 3418–3451 (2019)
125. H.J. Snaith, Present status and future prospects of perovskite photovoltaics. Nat. Mater. **17**, 372–376 (2018)
126. P. Gao, A.R.B.M. Yusoff, M.K. Nazeeruddin, Dimensionality engineering of hybrid halide perovskite light absorbers. Nat. Commun. **9**, 5028 (2018)
127. X. Zhang, L. Li, Z. Sun, J. Luo, Rational chemical doping of metal halide perovskites. Chem. Soc. Rev. **48**, 517–539 (2019)
128. J. Shamsi, A.S. Urban, M. Imran, L. De Trizio, L. Manna, Metal halide perovskite nanocrystals: synthesis, post-synthesis modifications, and their optical properties. Chem. Rev. **119**, 3296–3348 (2019)
129. A. Babayigit, A. Ethirajan, M. Muller, B. Conings, Toxicity of organometal halide perovskite solar cells. Nat. Mater. **15**, 247–251 (2016)
130. P. Wu, S. Wang, X. Li, F. Zhang, Beyond efficiency fever: preventing lead leakage for perovskite solar cells. Matter **5**, 1137–1161 (2022)
131. Y. Yan, T. Pullerits, K. Zheng, Z. Liang, Advancing tin halide perovskites: strategies toward the ASnX$_3$ paradigm for efficient and durable optoelectronics. ACS Energy Lett. **5**, 2052–2086 (2020)

## Publisher's Note